Experimental study of the fracture kinetics of a tubular 16MnNiMo5 steel specimen under biaxial loading at 900 and 1000 °C

Nicolas Tardif, Michel Coret, Alain Combescure

Experimental study of the fracture kinetics of a tubular 16MnNiMo5 steel specimen under biaxial loading at 900 and 1000 °C. Application to the rupture of a vessel bottom head during a core meltdown accident in a pressurized water reactor

N. Tardif[a,b], M. Coret[b], A. Combescure[b]

[a] *ISRN, BP17 92262 Fontenay-aux-Roses Cedex, France*
[b] *Université de Lyon, CNRS, INSA-Lyon, LaMCoS, UMR5259, 20 avenue Albert Einstein, F69621 Villeurbanne Cedex, France*

This study proposes an experimental analysis of the creep, crack initiation and crack propagation phases in a 16MnNiMo5 steel subjected to thermomechanical loading representing a core meltdown accident in a pressurized water reactor involving the transfer of a molten corium bath to the bottom head. The experimental setup enabled a biaxial mechanical loading (internal pressure + tension) to be applied to a tubular specimen at 900 and 1000 °C. In addition to the usual temperature, load, displacement and pressure measurements, the specimen was observed by two high-speed numerical cameras and an infrared camera. The crack's initiation and propagation conditions and the depressurization law were inferred from these measurements. At such temperatures, creep induces very large strains prior to the occurrence of the cracks which, in the worst-case scenario, can propagate at velocities as high as several meters per second. The design of the experiment enabled us to study the influence of the temperature (magnitude and hoop distribution), of the toughness of the steel (two grades were studied) and of the volume of pressurized gas. The results show that creep and crack propagation are highly dependent on temperature, and also that crack initiation and propagation are highly dependent on the degree of heterogeneity which is responsible for the localized initiation of the crack.

1. Introduction

This study was undertaken in the context of problems raised by severe accidents in French pressurized water reactors. A severe accident is defined as one during which the fuel is significantly degraded due to the more or less complete meltdown of the core of the reactor. This is generally caused by insufficient cooling of the core, whose residual power generated by the radioactivity of the fission products accumulated in the fuel can no longer be evacuated. After one or several hours, following multiple human errors and/or material failures, the fuel elements begin to deteriorate. Then, a succession of numerous and complex phenomena takes place according to various scenarios which depend on the initial conditions and on the actions of the operators; these scenarios may eventually lead to the loss of integrity of the confinement and a risk of significant release of radioactive products outside of the confinement building.

More specifically, we are considering the case in which the degradation of the core leads to the transfer of a molten corium bath, which is a highly caloric mixture of an oxidized phase U-Zr-0 (the product of the melting of the Zircaloy of the cladding and the dissolution of the fuel) and a metallic phase derived from the structural materials of the core (steel, Inconel, etc.), toward the bottom head. At this point, the integrity of the vessel can be jeopardized due to various mechanisms. For example, during the flowing of the corium to the bottom head, the vessel can become eroded by direct contact with the molten corium flow or damaged by a possible steam explosion when the corium interacts with the residual liquid water in the bottom head. Besides, even if the vessel successfully survives that transient flow phase, it can subsequently experience creep rupture when the corium bath settles to the bottom head.

Even though such a scenario is highly improbable, the corresponding risks call for an improved prediction of each critical phase of the accident being considered in order to develop effective management strategies. In our research, the key point was the prediction of the initiation and propagation of the crack due to creep. Indeed, the time of occurrence, the position and the final size of the

breach are determining factors of the external consequences of the accident.

The physical variables which influence the time of rupture of the vessel are mainly the primary pressure and the temperature distribution in the vessel. Generally, the primary pressure in the vessel is uniform (minimum 0.9 MPa if the safety valves are activated), with peaks in the case of water injection. The temperature of the bottom head is highly dependent on the thermal flow dispersed through its thickness. Thus, proper modeling of the composition of the corium is necessary in order to determine the temperature boundary conditions for the bottom head wall. This modeling still contains numerous uncertainties because it depends on the scenario being considered (Seiler et al., 2007; Bechta et al., 2008).

In our research, the range of temperatures being studied was chosen as a function of the data collected in the analysis of the TMI-2 accident which took place at the Three Mile Island power plant (OECD, 1993).The superficial temperature of the wall reached 1100 °C during 30 min with a gradient through the thickness of 2–4 °C mm^{-1} over an elliptical hot spot of 1 m × 0.8 m.

Very detailed experimental models reproducing the thermomechanical loading on reduced-scale bottom heads (LHF: Chu et al., 1998; Bucalossi, 2001a,b; OLHF: Bentz et al., 2000a,b Humphries et al., 2002; and FOREVER: Sehgal et al., 2003, 2005) pointed out a failure mode of the vessel by initiation of a localized crack and a great disparity in the sizes of this crack, even in the case of similar loading cases. An assumption concerning the influence of the variability of the fracture behavior of American pressure vessel steel at the temperatures being studied was formulated in order to explain these discrepancies (OLIS, 2002). Initially, however, this variability was not taken into account in the design of experiment of these programs.

French pressure vessel steel, which is close to American steel, also presents highly variable fracture behavior. Chemical and metallurgical experiments suggest that elements present as traces are responsible for that weakening, which is related to the combined effect of aluminum nitride AlN and manganese sulfide MnS precipitates. The former act by blocking the grain joints because they inhibit intergranular slippage and joint migration, and the latter constitute cavity germination and growth sites. This weakening depends primarily on the sulfur concentration of the steel grade, but also on the thermal history (initial grain size produced by possible thermal treatments (Sestier, 1998), testing temperature) and, sometimes, on the loading rate or on the stress applied for the creep tests. In the context of the thermal treatments applied during the manufacturing of the vessels, in-depth characterization of the behavior of two such steel grades was carried out both in healthy conditions (Vereecke, 2004; Gentzbittel et al., 2007; Gentzbittel and Calapez, 2008; Tardif, 2009) and at rupture (Nicolas et al., 2001; Koundy et al., 2008a,b; Tardif et al., 2010). The Ruptherr grade is ductile at high temperature for all test temperatures and rates of solicitation. Its damage mechanism is of the transgranular ductile type. Over a range of temperatures going from 900 to 1100 °C, the Krakatoa grade presents a ductility trough which is more or less pronounced depending of the solicitation rate (Fig. 3). Its damage mechanism is of the intergranular creep type.

The main objective of this paper is to present, for the steel grades mentioned previously, the results of simple, well-instrumented tests which, under the thermomechanical conditions of a severe accident, enable the characterization of not only the creep phases, but also the crack initiation and crack propagation phases. Indeed, these tests give an order of magnitude of the crack propagation velocity. Besides, the design of the experiment enables one to discriminate among the factors which have a first-order influence on the crack's propagation and tends to relativize the influence of the material's grade in the case of these structural tests.

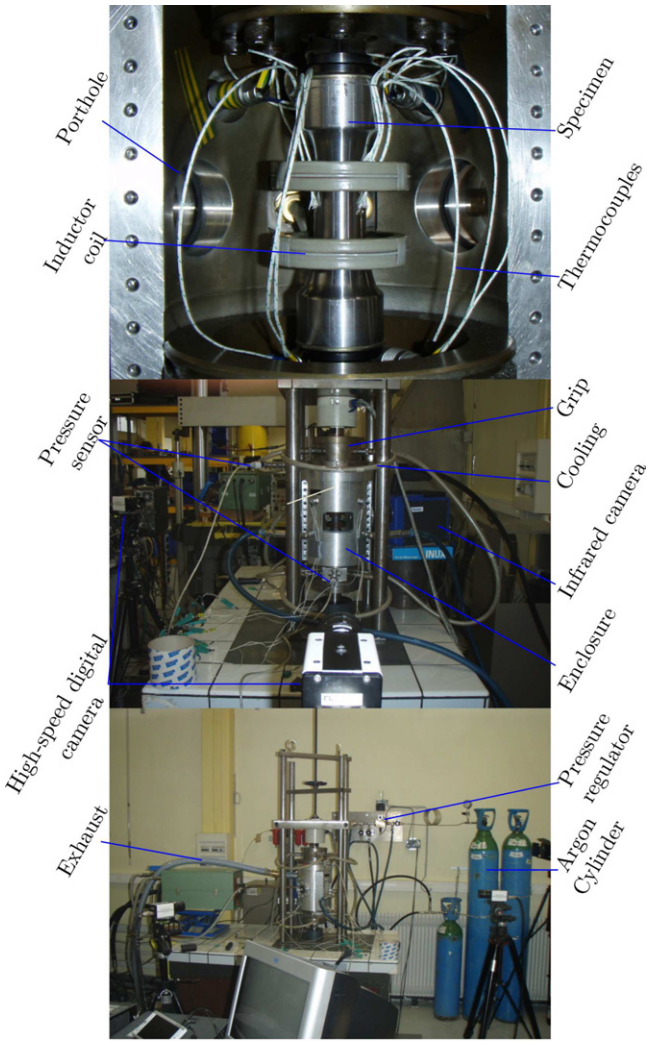

Fig. 1. The test bench.

The first part presents the test setup and the modeling choices which were made. The purpose of the second part is to study the details of an example of results in order to pinpoint the different phenomena observed experimentally. In the third part, the tests are discussed more globally, leading to the establishment of a hierarchy among the factors which influence the crack's propagation.

2. Choice of a model and description of the test setup

A description of the test setup is given in Fig. 1.

2.1. The test specimens

The geometry of the test specimen was axisymmetrical (Fig. 2). Such a shape enables one to adjust k (Eq. (1)), the biaxiality ratio of the stresses which occur in the gage length. (In the vessel case, this ratio varies between 1 in the bottom head and 2 in the cylindrical part.)

$$k = \frac{\sigma_I}{\sigma_{II}} \quad \text{with} \quad |\sigma_{III}| \ll |\sigma_I|, \quad |\sigma_{II}|, \tag{1}$$

where σ_i denotes the principal stresses.

The ratio of the radius to the thickness is close to the case of 1350 MW reactors, but the dimensions were drastically reduced for economic reasons. The thickness t in the gage length was 0.8 mm

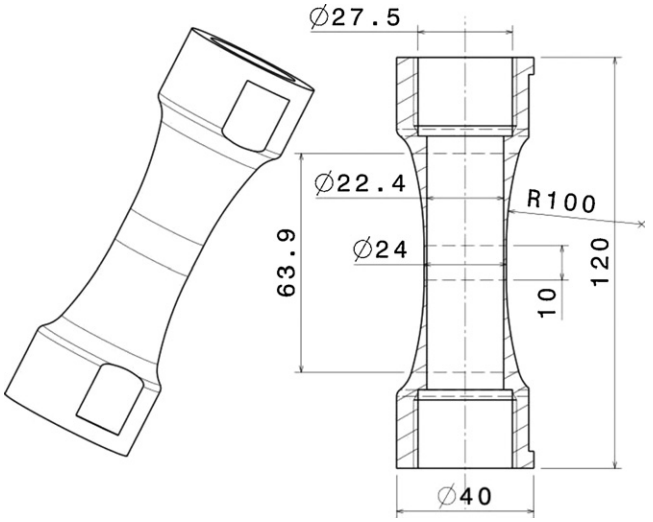

Fig. 2. A specimen.

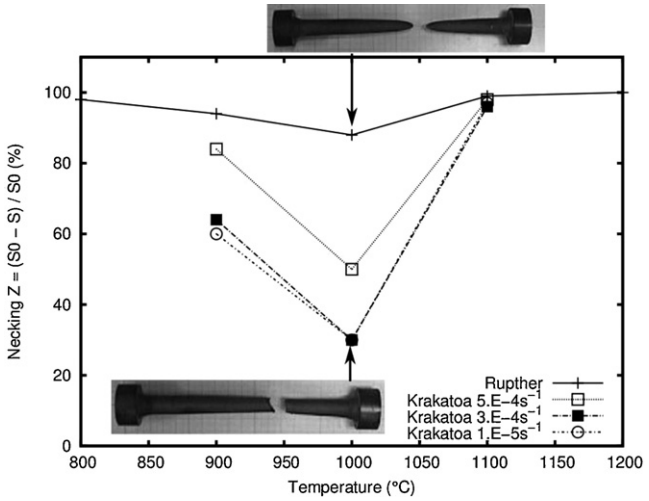

Fig. 3. Krakatoa and Rupther grades of 16MND5 steel, emphasizing the ductility trough (Gentzbittel et al., 2007).

(grain size about 0.02 mm), the outer radius R_{ou} was 12 mm and the height h was 10 mm.

The specimens were manufactured by turning and grinding-lapping from rough piping material set aside during the production of the vessels. Thus, the thermal treatments (which influence the fracture behavior of the steel grades) were respected. Two 16MnNiMo5 steel grades were studied: the Krakatoa grade, which presents a ductility trough between 900 and 1100 °C associated with a damage mechanism of the intergranular creep type, and the Rupther grade, which has a much less pronounced ductility trough associated with a transgranular ductile damage type (Fig. 3). The composition of these two grades is given in Table 1.

The thickness of the specimens in the gage length was controlled by scanning using a three-dimensional measuring machine with at least 3 latitudes and 4 points per measured latitude. The maximum thickness variation over a specimen's wall measured over the entire population was 0.037 mm.

The specimen were mounted in the machine, using a custom build clamping mechanism, including an enclosure in order to prevent possible projections of material during cracking.

2.2. The loading

2.2.1. Thermal loading

The heat flow produced by the molten corium bath was simulated by induction heating of the gage length of the specimen. Two inductor geometries were used (Fig. 4). Inductor 2 provided a uniform temperature in the gage length of the specimen, whereas Inductor 1 produced a non-uniform distribution with a hot spot near the junction of the air gap of the coil (Fig. 5). Heat was applied using a 6 kW power generator with a water-cooled power source.

The temperature distribution in the gage length was measured by three spot-welded type-K thermocouples, one of which was used for feedback-control. Six other thermocouples were welded over half the height of the specimen. The measurement uncertainty was 1.4% of the measured value. Besides, the temperature distribution was measured using an infrared camera. Two sapphire windows were added to the enclosure in order to enable this measurement. A graphite paint was used for the 900 °C tests in order to ensure constant emissivity in the gage length. This apparatus could not be used for the 1000 °C tests, resulting in a less reliable measurement. The atmosphere of the enclosure was swept with argon prior to the test in order to avoid any oxidation development over

Table 1
Chemical analysis of the two 16MND5 pressure vessel steel grades, in thousandths of % mass (the balance being iron).

C	Si	Mn	P	S	Ni	Cr	Mo	V	Cu	Al	Co	Nb	B	H (ppm)
Krakatoa														
140	160	1.310	10	7	790	190	490	7	50		10			
Rupther														
170	250	1.440	4	2	750	200	510	4	10	16	4	1	0.1	0.9

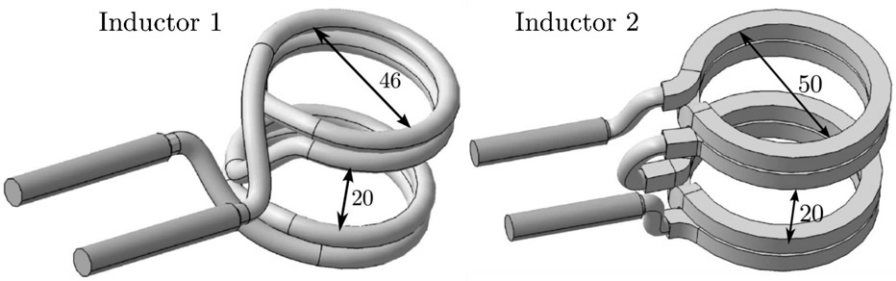

Fig. 4. Inductor.

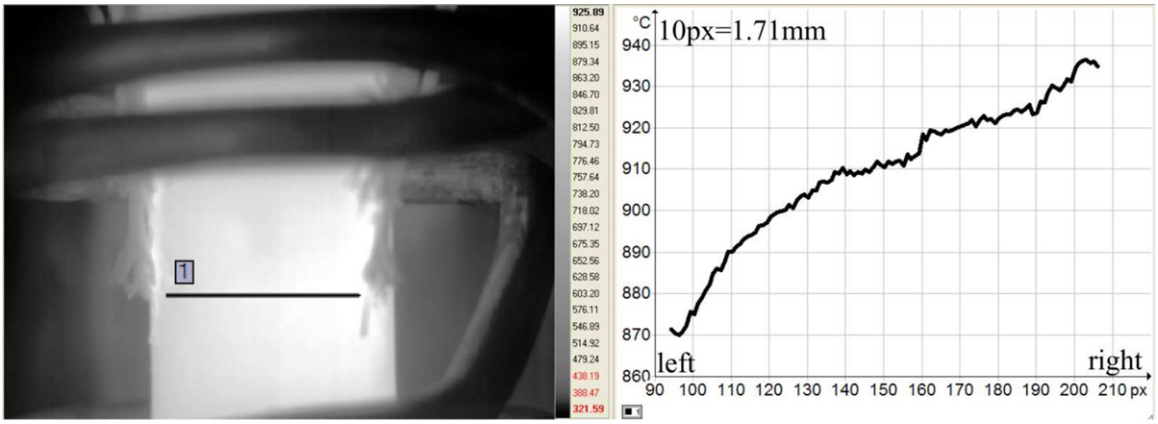

Fig. 5. Temperature distribution obtained with Inductor 1.

the surface of the specimen, which could have impaired the optical monitoring of the crack's propagation.

2.2.2. Mechanical loading

The stress state of the vessel is biaxial. The initial biaxiality ratio varies between 1 and 2 depending on the latitude being observed. This loading was reproduced by subjecting the specimen to tension and internal pressure. The tests were carried out at a pressure p equal to 2.4 MPa (moderate pressure in the vessel) and a biaxiality ratio k equal to 1.65. The axial stress σ_{zz} was greater than the hoop stress $\sigma_{\theta\theta}$ in order to enforce a crack propagation in a plane orthogonal to the axis of the specimen.

The specimen was pressurized with argon. The gas source was a 50 L bottle loaded at 20 MPa. This bottle was connected to an electrically activated proportional regulator. The pressure was servo-controlled over a 0–4 MPa range. The pressure information was acquired as close as possible to the gage length of the specimen using 2 pressure sensors located on the upper (p_{sup}) and lower (p_{inf}) clamping mechanisms of the tensile machine.

The tensile load was the sum of two contributions:

- A load applied by a 10 kN hydraulic tensile machine with servo-control based on the load. The custom build clamping mechanisms were water-cooled. The force F was acquired through a 10 kN range load cell, and the displacement v_{ll} of the hydraulic actuator was acquired through the machine's LVDT sensor. (No local measurement of the strains in the gage length was implemented, but the stiffness of the water-cooled clamping mechanism and the machine was very high compared to that of the specimen at 900–1000 °C.) The measured load F includes a component due to friction of a joint positioned between the enclosure, mounted on the upper clamping mechanism connected to the load cell and the lower clamping mechanism connected to the hydraulic actuator of the machine. This component was not constant because the joint, being positioned in a groove, first rolled without friction, then was subjected to friction once it was blocked by the groove's side. This resulted in an uncertainty about the magnitude of the load F.
- A tension due to the end loading induced by the pressure. This tension was not measured by the load cell.

Thus, the nominal stresses can be written as:

$$\sigma_{\theta\theta} = p_{inf}\frac{R_{in}}{t}, \tag{2}$$

$$\sigma_{zz} = \frac{\pi p_{inf} R_{in}^2 + F}{\pi(R_{ou}^2 - R_{in}^2)}, \tag{3}$$

where p_{inf} denotes the pressure measured at the lower clamping mechanism, F the load measured by the load cell of the tensile machine, R_{in} the inner radius, and R_{ou} the outer radius. One should note that for a given pressure the geometry of the specimen leads to a stress state higher than that of the vessel. Thus, the initial state of the tests corresponds to a state in which the vessel would have already begun to creep.

In order to relate the volume of gas available for the loading to reality, we compared the ratio of the energy contained in the volume of pressurized gas to the fracture energy necessary for the complete hoop failure of the structure, leading to Eq. (4):

$$\frac{p_s V_s}{G_c t_s a_s} = \frac{p_v V_v}{G_c t_v a_v}, \tag{4}$$

where p denotes the pressure, V the volume, G_c the energy release rate, t the thickness, and a the crack's length corresponding to the complete hoop failure of the structure. Indices s and v correspond to the specimen and the vessel, respectively.

For a similar pressure, neglecting the temperature gradient through the thickness of the vessel's wall and setting a latitude corresponding to a 1-m radius, one gets a representative volume V_s^r approximately equal to 24 dm^3. Two extreme cases were studied in order to quantify the influence of that volume: a very small volume (0.4 dm^3) and a quasi-infinite volume.

The loading schedule is described in Fig. 6. First, a sweeping phase of the protective enclosure's atmosphere was carried out. Then, the temperature setting was applied at a rate of 150 °C min^{-1} under zero load. The specimen was subjected to mechanical loading only after the temperature plateau was reached. The load and pressure were kept constant until the rupture of the specimen.

2.3. Monitoring of the crack's propagation

Monitoring of the crack's propagation was achieved thanks to an infrared camera (acquisition frequency 177fs^{-1}, resolution 320 px × 256 px) and two high-speed numerical cameras (acquisition frequency 1000fs^{-1}, resolution 400 px × 400px). The cameras were arranged so that the whole circumference of the specimen could be seen. Visualization was made possible by adding windows to the enclosure.

The image acquisition process was synchronized with all the other measurements through a trigger. Then it was possible to obtain the crack's velocity and the cracked area simply by using image processing.

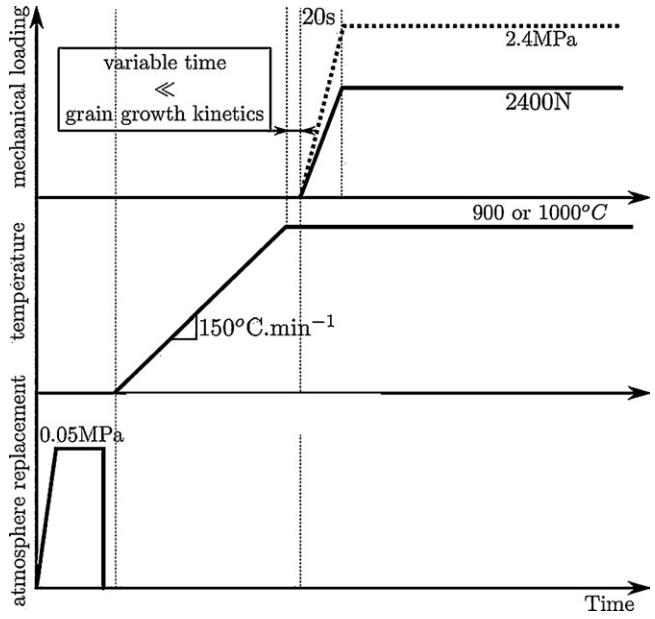

Fig. 6. The test schedule.

Table 2
Design of the experiment.

Temperature (°C)	900	900	1000
Volume (dm^3)	0.4	∞	0.4
Inductor	1	2	2
Grade	Krakatoa		
Specimen's ID	F, H	Y	E, I
Grade	Rupther		
Specimen's ID	B, D	X	K, M

2.4. Design of the experiment

The design of the experiment, given in Table 2, was devised so that the influence of the steel grade, of the temperature and of the loading volume could be studied.

3. Description of the phenomena involved – example of results

The test described in this section, performed at 1000 °C on the Rupther grade using Inductor 2, corresponds to Specimen M. The positioning of the cameras and thermocouples is shown in the top view of the specimen and induction coil of Fig. 7. Regarding angular positioning, the thermocouples were set along 3 generatrices ($\theta = \{0, 120, 240\}$).

The temperature profile along the half-height of the specimen at the beginning of the mechanical loading is shown in Fig. 8. In the gage length ($z = \pm 5$ mm), the temperature was homogeneous and the maximum difference measured until the initiation of the crack over the entire set of tests carried out with that inductor was 40 °C. The temperature varied linearly with the distance from the induction coil's air gap. The slope of that straight line decreased with time because of thermal conduction.

A similar temperature profile was observed for Inductor 1, with the hoop variation in the gage length shown in Fig. 5.

The mechanical loading applied to the specimen in terms of nominal stresses (Eqs. (2) and (3)) is shown in Fig. 9. The displacement v_{ll} of the hydraulic actuator is shown on the same graph. A zoom of the mechanical loading at the moment of the crack's propagation is shown in Fig. 10. Plots of the deformed shapes and of the

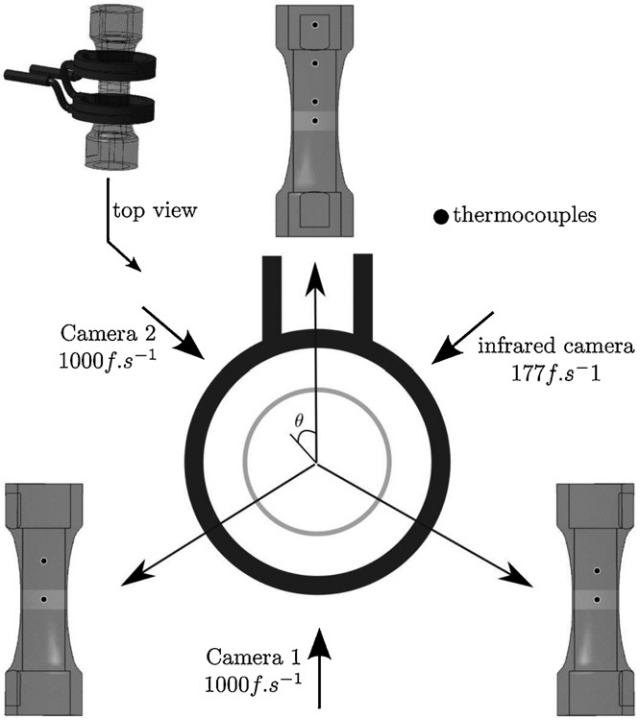

Fig. 7. Positioning scheme for the test.

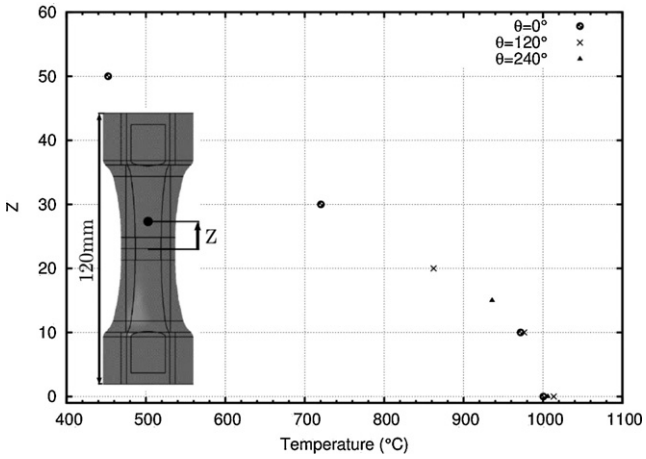

Fig. 8. Temperature profile at the beginning of the mechanical loading.

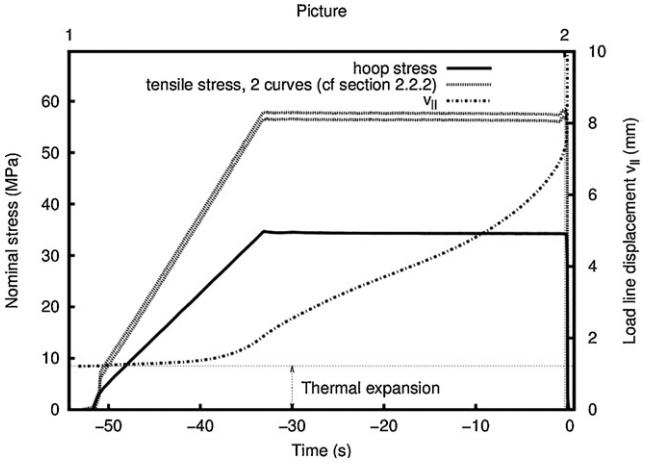

Fig. 9. The mechanical loading.

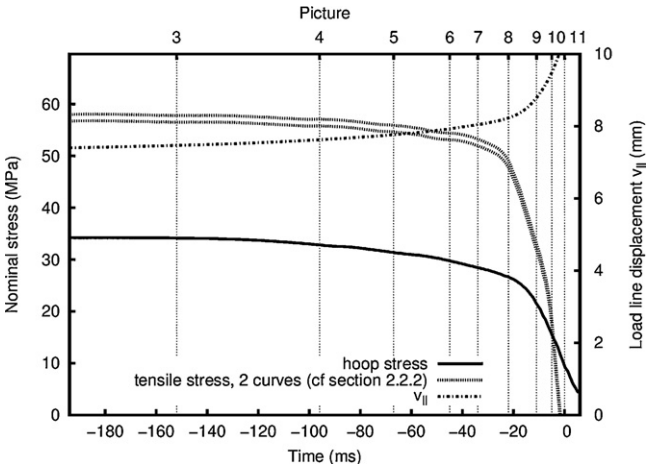

Fig. 10. The mechanical loading – zoom on the crack.

crack's propagation are shown in Fig. 11. The arrangement of these graphs corresponds to the time stamp associated with each picture of Fig. 11.

The biaxial creep loading induced a longitudinal strain and a barreling in the gage length. These strains followed the three characteristic stages of creep. During the test being considered, the loading lasted about 50 s prior to the complete rupture of the specimen.

In the tertiary creep stage, one could observe a localization of the strains and damage leading to a local initiation of a crack. This localization took place in a zone where the ultimate stress was reached. It could be the result of several types of heterogeneities: a hot spot tending to lower the ultimate stress of the material and promote creep; a higher stress induced by a slight bending of the specimen due to its mounting or by a variation in the thickness of the wall which became overstressed due to the pressure; or a metallurgical defect, etc.

The initiation of the crack led to the release of the pressurized gas contained in the specimen. This release caused local cooling of the lips of the crack (see the local change of color near the lips of the crack in Fig. 11). The size of the cooled zone and the temperature drop are functions of the fracture kinetics. These data are quantified in Fig. 12 for the tests at 900 °C (slow fracture kinetics) and in Fig. 13 for the tests at 1000 °C (fast fracture kinetics). Besides, the depressurization led to a decrease in the hoop stress $\sigma_{\theta\theta}$ and in the part of the axial stress σ_{zz} due to the pressure end loading (Fig. 10).

This cooling tended to reinforce the properties of the material locally by increasing the ultimate stress. Thus, the crack's propagation was stopped. Then, a new localization took place in a different zone (e.g. times 3 and 4 in Fig. 11). Consequently, the increase in the cracked area was induced by multiple initiations of cracks in combination with one another rather that by the propagation of a crack

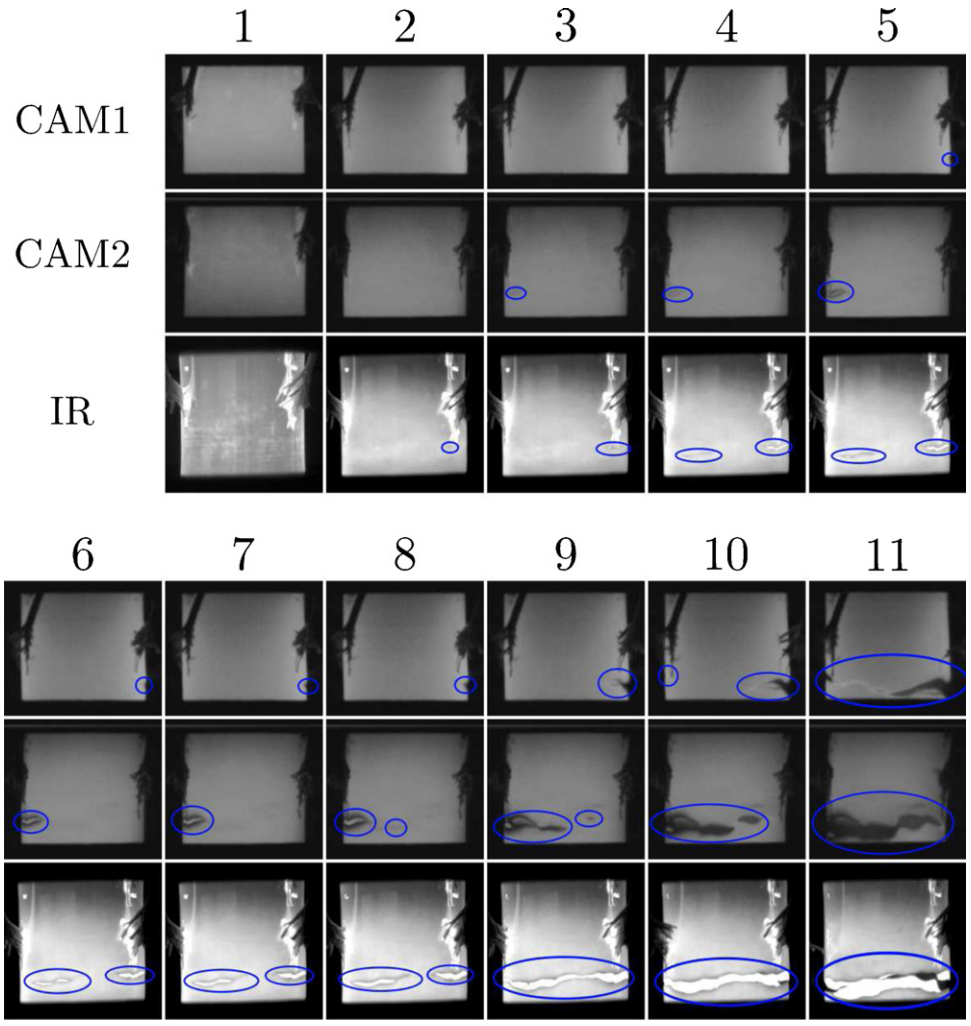

Fig. 11. The crack's propagation in pictures.

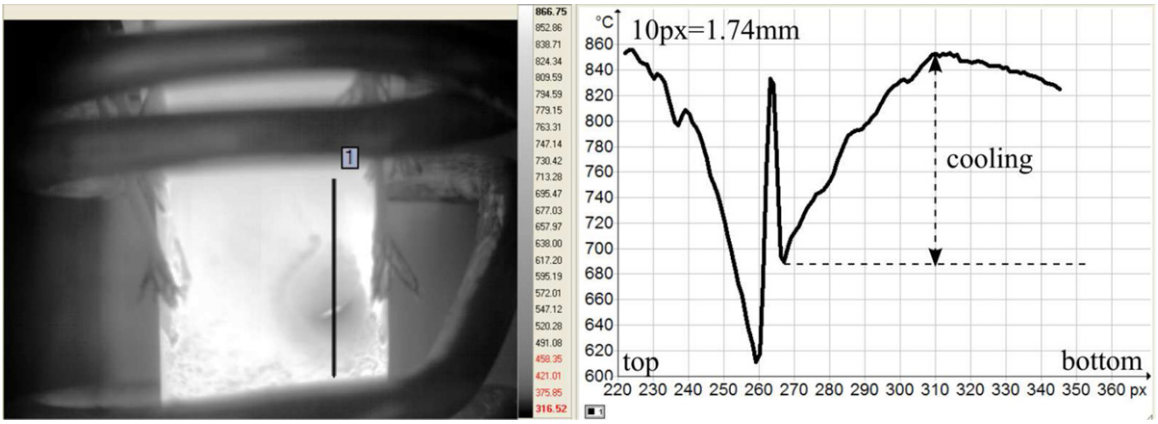

Fig. 12. Cooling of the crack's lips during the 900 °C tests.

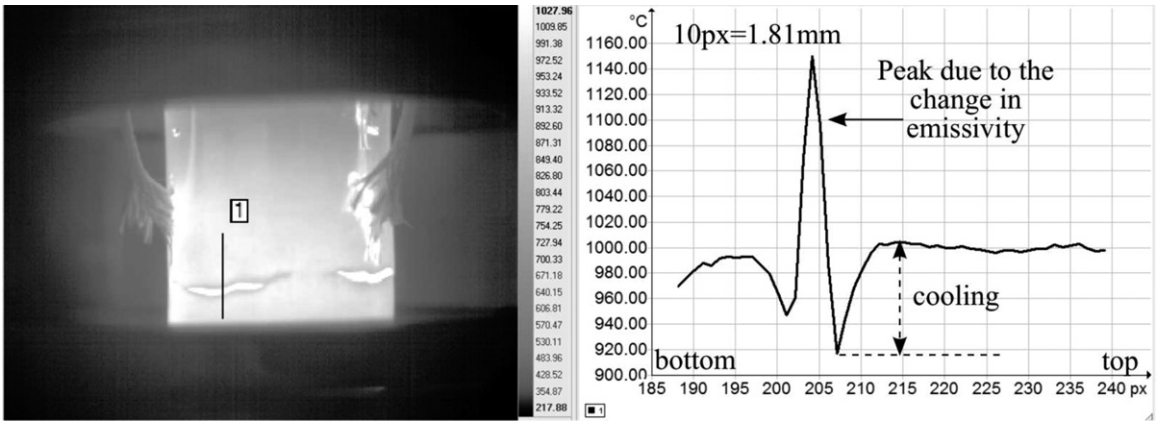

Fig. 13. Cooling of the crack's lips during the 1000 °C tests.

issued from a single initiation. While each initiation took place in a plane normal to the axis of the pipe, all of them did not necessarily occur at the same latitude. Thus, the crack's path was not always coplanar, which could have had an influence on the crack's propagation velocity.

The crack's propagation (Fig. 14) followed two phases. Initially, the propagation was stable because the work of the external forces was converted into viscoplastic strain energy and surface energy stored at the crack's lips. Thus, in the case of test M, the propagation occurred at about 30 mm s^{-1}, then it accelerated to end up in an unstable phase. In that second phase, an important part of the work of the external forces was converted to acceleration and the crack's propagation velocity reached 2 m s^{-1}. The transition between the two phases is made visible in Fig. 10 by the decrease in the load carrying capacity of the specimen.

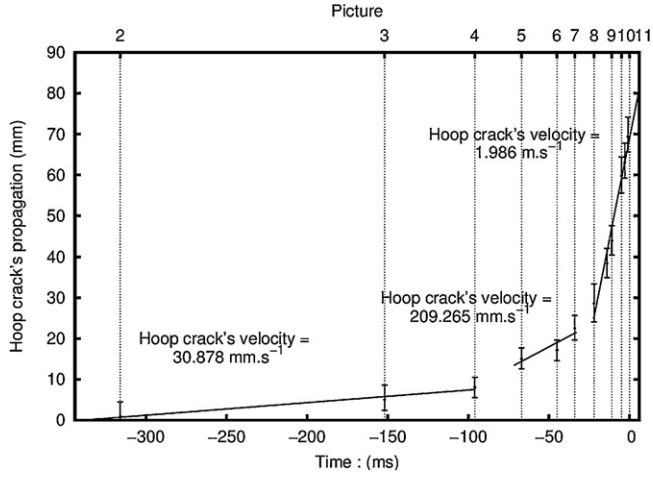

Fig. 14. Hoop propagation of the crack.

Finally, image processing made the area of the cracked surface accessible at each instant. Then the experimental depressurization p_{exp} could be represented correctly by a simple adiabatic depressurization law taking into account the head loss in the pneumatic circuit (Fig. 15):

$$\dot{p}_{calc} = p_{calc}\frac{2\gamma}{1-\gamma}\frac{QS}{1+QSt}, \tag{5}$$

with

$$Q = \frac{\gamma-1}{2}\frac{\Gamma}{\beta}, \tag{6}$$

$$\Gamma = \left(\frac{2}{\gamma+1}\right)^{(\gamma+1)/(2(\gamma-1))}, \tag{7}$$

and

$$\beta = \frac{V}{\eta\sqrt{\gamma\chi T}}, \tag{8}$$

where p_{calc} refers to the pressure, t to time, S to the cracked area, V to the volume of pressurized gas and T to the temperature of the gas. The constants γ, η and χ represent respectively the exponent of the ideal gas law (1.66), the head loss coefficient of the circuit and the ratio of the constant 8314 to the atomic mass of argon (40).

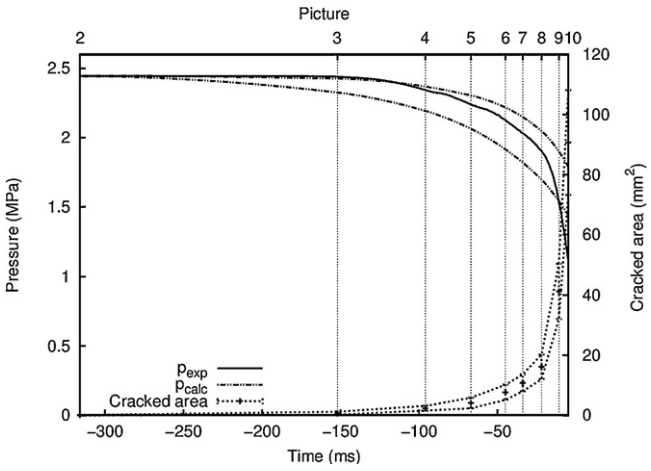

Fig. 15. The depressurization law.

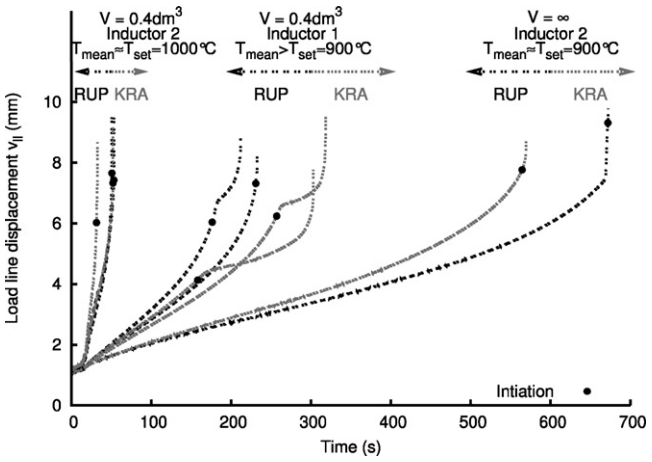

Fig. 16. Load line displacement versus time for each test.

4. Interpretation of the results in relation to the design of the experiment

4.1. Creep

Fig. 16 represents the axial displacement response of the whole set of tests which were carried out. One can easily distinguish three groups, which correspond to the three sets of parameters relative to the temperature of the design of experiment: {1000 °C, Inductor 2}, {900 °C, Inductor 1}, and {900 °C, Inductor 2}. The grey curves correspond to the Krakatoa grade and the black curves correspond to the Rupther grade.

The three groups of curves indicate a significant influence of the temperature. Indeed, the temperature measured by the three thermocouples in the gage length is represented by the histogram of Fig. 17. The three levels of the histogram correspond to the minimum temperature, the maximum temperature and the average temperature over all the acquired points. These three values were obtained for the points situated between the beginning of the mechanical loading and the initiation of the crack. The hollow histograms correspond to the Rupther grade and the solid histograms correspond to the Krakatoa grade.

The strain rate for the same mechanical loading was much higher for the K, M, E and I tests (Inductor 2: 1000 °C) than for the X and Y tests (Inductor 2: 900 °C).

The B, D, F and H tests were carried out for a set point of 900 °C with Inductor 1. The measurements show the hot spot at the 0 angular position. Thus, these tests were performed at an average temperature over the circumference (T_{mean}) which is greater than the set temperature (T_{set}) (Fig. 5), which explains that the strain rate in these tests was greater than in the tests at 900 °C with Inductor 2.

Each group of curves presents a disparity in the results concerning creep, which can also be related to the temperature. For example, test E departs from tests K, M and I because of a greater average temperature. Let us recall that the uncertainty of the thermocouples was 1.4% of the measured value.

As expected, we could observe no influence of the steel grade on creep. Indeed, the chemical elements present as traces (aluminum nitride AlN and manganese sulfide MnS precipitates) whose proportion defines the grades, are preferential sites for the damage initiation (void nucleation). However, they have little influence on

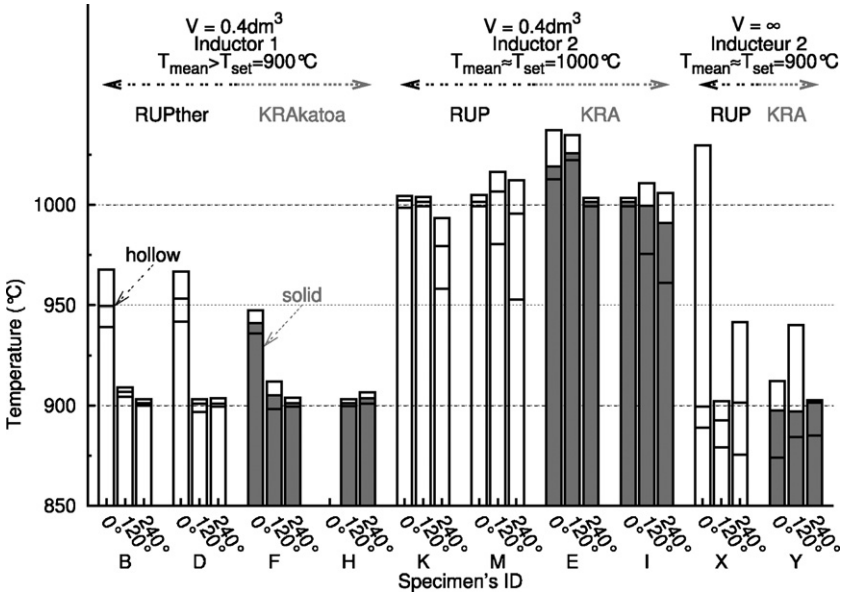

Fig. 17. Temperature measured by the thermocouples in the useful zone: maximum value, mean value and minimum value calculated from the beginning of the loading to the initiation of the crack for each test.

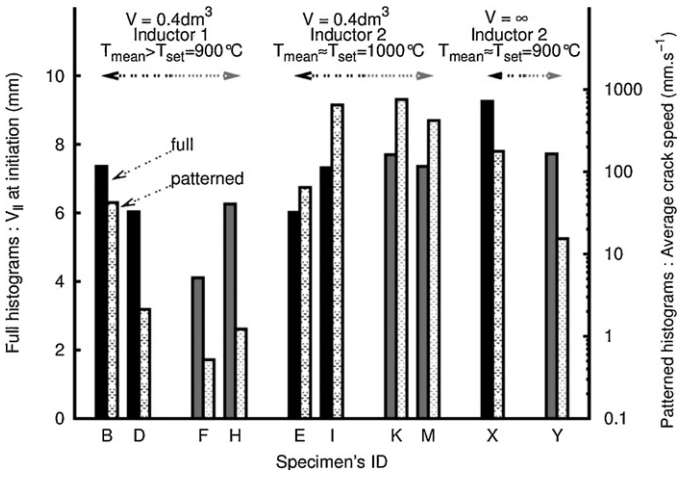

Fig. 18. Correlation between v_{ll} at initiation and the mean propagation velocity of the crack.

the viscoplastic behavior as they do not disturb the diffusive phenomena and the dislocation mechanisms, at least during the first stage of creep. The volume of pressurized gas has also no influence on creep because the volume variation caused by the viscoplastic deformations of the specimen was negligible compared to the initial volume (even in the case of a 0.4 dm^3 volume). Thus, there was no coupling between creep and the prescribed pressure (Fig. 9).

4.2. Initiation of the crack

The initiation of the crack, measured visually, was correlated at the beginning of the depressurization. The initiation is represented by a point on the curves of Fig. 16. The magnitude of the axial displacement of the hydraulic actuator at initiation is shown in the full histograms of Fig. 18.

No influence of the temperature or of the steel grade is noticeable from the point of view of the results in terms of displacements at the initiation of the crack. The initiation is localized and is the result of a heterogeneity (hot spot, slight bending of the specimen due to the mounting, thickness, metallurgical defect, etc.) Indeed, one can observe that the displacement at initiation was, on the average, less for the tests carried out with Inductor 1, which generates a hot spot, than for the tests carried out with Inductor 2.

4.3. Propagation of the crack

The mean propagation velocity of the crack, shown in Fig. 18 by the patterned histograms, represents the ratio of the initial circumference of the specimen to the total cracking time.

4.3.1. Influence of the temperature

Histogram 18 shows a dependency on the testing temperature. The mean crack propagation velocity was higher in the case of the tests at 1000 °C than in the case of the tests at 900 °C, even when the tests were carried out with the same inductor (which, therefore, had the same degree of thermal heterogeneity). If one considers more specifically the crack propagation velocities during the stable and unstable phases, one can observe that the influence of the temperature was high in the stable phase. During that phase, the hoop crack propagation velocities ranged from 0.1 to 50 mm s^{-1} at 900 °C, while they ranged from 10 to 500 mm s^{-1} at 1000. During the unstable phase, no trend can be seen, with crack propagation velocities ranging between 1 and 10 m s^{-1}.

4.3.2. Influence of the steel grade

As in the case of the displacement at initiation, the steel grade had no significant influence on the results in terms of crack propagation velocity. Nevertheless, differences concerning damage can be observed by scanning electron microscopy at the level of the rupture pattern and of the internal surface in the gage length.

Fig. 19 shows the surface state of the internal wall of the gage length. Microcracks can be observed very clearly at 900 °C for the Krakatoa grade. Some initial microcracking is noticeable at 1000 °C for the same grade. The internal wall of the Ruptther grade is much smoother at both temperatures. Fig. 20 shows rupture surfaces involving two localized mechanisms: a high strain and the presence of void cavities. At the same temperature, the Krakatoa grade presents a larger number of void cavities and less localized necking than the Ruptther grade, which agrees with the observations of Gentzbittel et al. (2007) and confirms the relative brittleness of the Krakatoa grade compared to the Ruptther grade, but these phenomena seem to influence the crack's propagation in the context of our tests only to the second order.

Therefore, an alternative explanation must be sought for the dispersion of the crack's propagation observed in our tests as well as in other test programs concerned with the same issue (Bentz et al., 2000a,b; Humphries et al., 2002; Sehgal et al., 2003, 2005).

4.3.3. Influence of the heterogeneity responsible for the localization

By comparing the crack propagation velocities to the displacement at the beginning of the crack using Histogram 18 for each set of parameters of the design of the experiment, one can observe that the earlier the initiation from the point of view of the displacement at initiation, the lower the crack propagation velocity. Thus, the larger the mean thinning of the wall of the gage length at initiation, the faster the crack's propagation. Besides, on average, the crack's propagation velocity for the tests carried out at 900 °C was less with Inductor 1 (hot spot) than with Inductor 2. This enabled the results in terms of the crack's propagation velocity to be correlated with the amount of heterogeneity responsible for its initiation.

Assuming a perfectly homogeneous material, perfect geometry and perfectly axisymmetrical loading, the plastic instability would occur homogeneously at the points of the gage length where the equivalent stress or the diffuse damage is maximum. All the points would crack simultaneously. Thus, the crack propagation velocity would be infinite.

In reality, there is a loss of axisymmetry due to some heterogeneity. During the creep phase, the specimen undergoes deformation and damage more or less uniformly depending on the level of heterogeneity, resulting in both localized plastic instability and localized damage then, subsequently, localized initiation of a crack.

Turner and Kolednik characterized a crack's propagation within an inelastic material by its energy dissipation rate R (Turner and Kolednik, 1994; Stampfl and Kolednik, 2000), which is an extension of the definition of toughness proposed by Griffith (1920). The apparent toughness R represents the dissipated energy which is necessary for the extension of a cracked surface $d\mathcal{A}$ (Eq. (9), Fig. 21). It can be viewed as the sum of two contributions: a volume dissipated energy dU_{un} (consisting of viscoplastic dissipation and dissipation by diffuse damage) and a surface dissipated energy which is responsible for the creation of the lips of crack Γ_0 (high strain and localized damage occuring in the fracture process zone):

$$R = \frac{d(U - U_e)}{d\mathcal{A}} = \frac{dU_{un}}{d\mathcal{A}} + \Gamma_0, \tag{9}$$

where U corresponds to the internal energy and U_e to the elastic energy.

Let us now consider the two cases of an early initiation and a late initiation (Fig. 21). The average deformation and the average

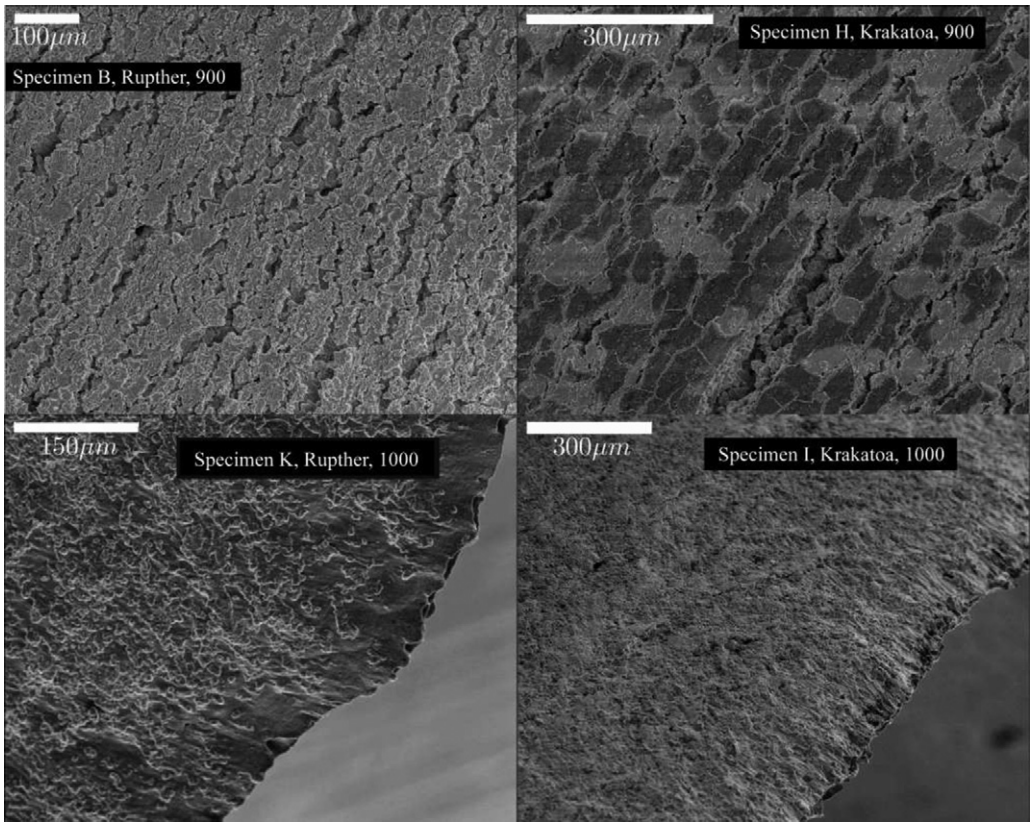

Fig. 19. Comparison of the superficial damage states of the internal wall of the gage length – images obtained by SEM.

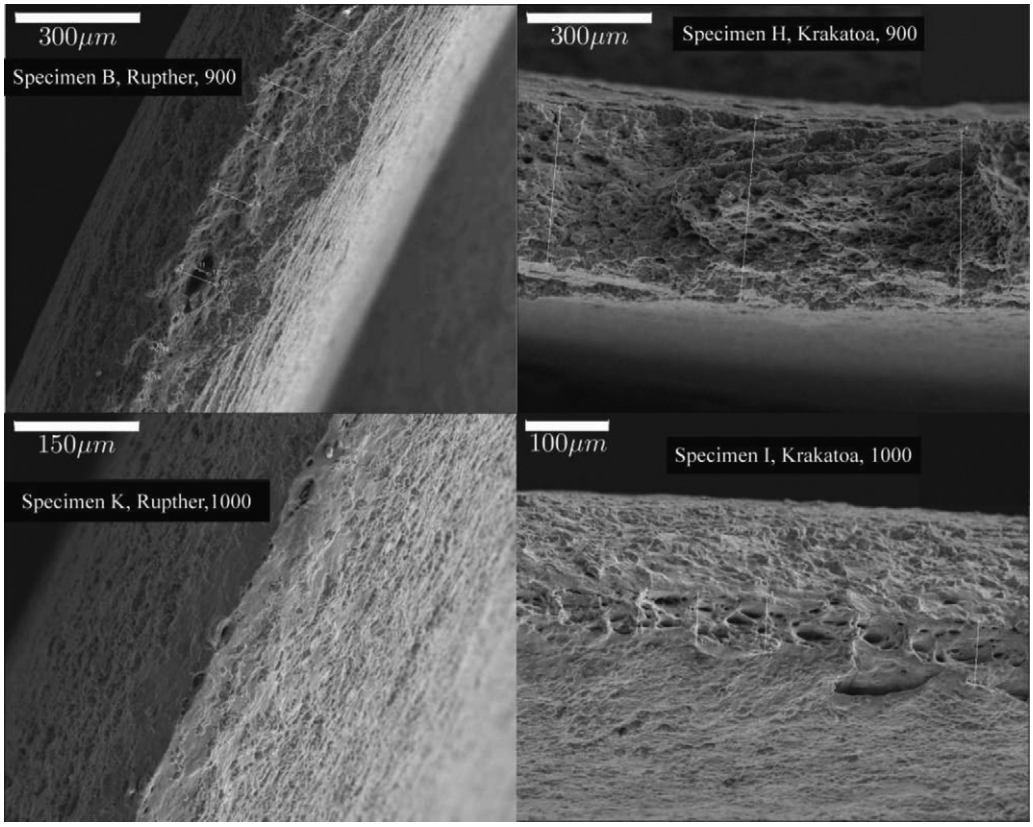

Fig. 20. Comparison of the rupture surfaces obtained by SEM.

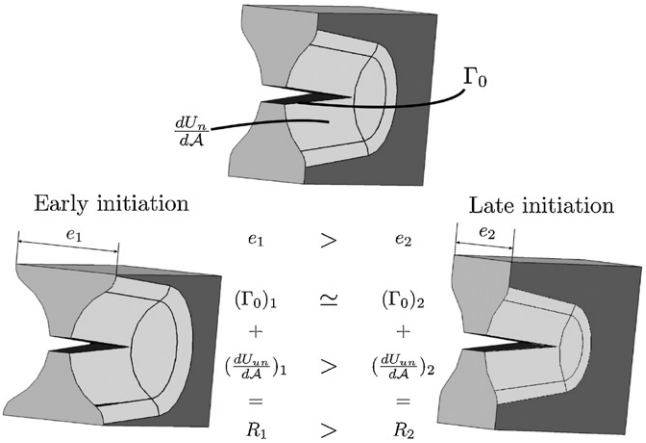

Fig. 21. The assumption on the influence of the initial defect.

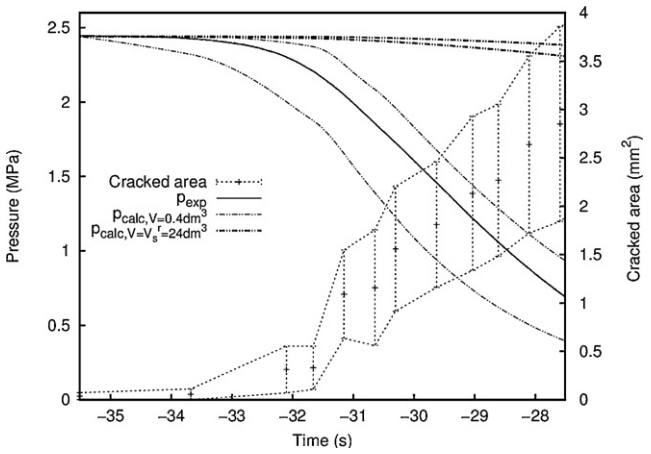

Fig. 22. Specimen D: the depressurization correlated with the cracked area.

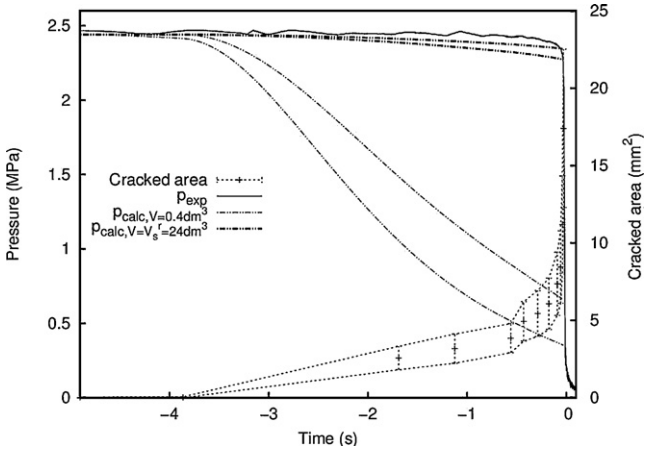

Fig. 23. Specimen Y: the depressurization correlated with the cracked area.

diffuse damage of the uncracked wall of the gage length are less in the case of high heterogeneity (early initiation) than in that of low heterogeneity (late initiation). Thus, assuming that the surface energy release rate Γ_0 is the same in both cases (an assumption which must be put into perspective considering the dependence of Γ_0 on the propagation velocity), the volume energy which must be dissipated inelastically to extend the crack $dU_{un}/d\mathcal{A}$ is much higher in the case of an earlier localization. Therefore, the crack's propagation is slower.

Furthermore, in our case, the depressurization induced by cracking affects the mechanical loading and causes local cooling of the crack's lips. These two phenomena tend to amplify the effect of heterogeneities.

4.3.4. Influence of the volume of pressurized gas

The volume of pressurized gas influences depressurization. In the case of the vessel, the internal pressure was the only contribution to the mechanical loading. In our tests, the depressurization resulted in a decrease in the hoop stress $\sigma_{\theta\theta}$ down to zero and a decrease in the axial stress σ_{zz} down to the value due to the force prescribed by the tensile machine. Thus, in order to conclude regarding the influence of the volume of pressurized gas, one must compare the depressurization kinetics to the fracture kinetics. For the tests carried out with a 0.4 dm^3 volume at 1000 °C, the fracture kinetics was high compared to the depressurization kinetics; therefore, the volume of gas was of little influence. Conversely, at 900 °C, the fracture kinetics was slow and the structure became completely depressurized before the complete separation of the structure. The consequence was a decrease in the axial velocity of the hydraulic actuator of the tensile machine (Fig. 16) which must be correlated with the decrease in the mechanical loading.

Thus, in order to quantify the influence of the volume of pressurized gas on the crack's propagation, one can compare the case of test D, performed at a low volume, with that of test Y, performed at a volume considered to be infinite. Figs. 22 and 23 show the depressurization observed in both tests. This depressurization is compared to that calculated for the volume $V = 0.4\,\mathrm{dm}^3$ and the representative volume $V_s^r = 24\,\mathrm{dm}^3$.

In the case of test D, the depressurization led to a decrease in the creep rate (Fig. 16), which, after depressurization, was caused solely by the axial force applied by the tensile machine. Thus, this modification of the mechanical loading resulted in a slowing down of the stable propagation of the crack. In reality, cracking would have completely stopped.

Specimen Y was subjected to a depressurization which was much more representative of reality. There was no decrease in creep rate. The crack progressed continuously until the unstable phase of the propagation.

Nevertheless, it remains difficult to quantify the influence of the volume of pressurized gas because while the two tests (Inductor 1 for Specimen D and Inductor 2 for Specimen Y) did not have the same heterogeneity ratio, after Specimen D had been completely depressurized there was no more local cooling of the crack's lips which tended to slow down its propagation.

5. Conclusion

A simplified experimental model was implemented in order to study the creep, crack initiation and crack propagation phases in the bottom head of a 1350 MW pressurized water reactor subjected to thermomechanical loading representing a core meltdown accident involving the transfer of a highly calorific corium bath to the bottom head.

The simplified model relies on the following aspects:

- Equivalence of the material's behavior.

Two 16MnNiMo5 steel grades were tested: the Rupther grade (ductile at high temperature) and the Krakatoa grade (more brittle at high temperature).

- Equivalence of the dominant geometric parameter.

In the tubular specimen, the ratio of the radius to the thickness was similar to that of the hemispherical bottom head.

- Equivalence of the stress state.

The specimen was subjected to a biaxial loading whose biaxiality ratio corresponded to rupture at a latitude near the cylindrical part of the vessel. The equivalent stress corresponded to a state in which the bottom head starts to creep as the result of a moderate 2.4 MPa internal pressure.

- Application of a thermal loading with a magnitude similar to that of the TMI-2 case.

The design of experiment made it possible to study the influence of temperature (distribution and magnitude), the influence of the 16MnNiMo5 steel grade and the influence of the volume of pressurized gas on the creep, crack initiation and crack propagation phases.

The results indicated the following trends:

- *Creep*: High influence of the temperature. The displacement velocities of the hydraulic actuator due to creep were approximately 12 times higher at 1000 °C than at 900 °C (with the same inductor).
- *Initiation of the crack*: Only the temperature distribution influences the displacement at the initiation of the crack. By extension, the initiation is due to a heterogeneity regarding the loading (either mechanical or thermal), a structural heterogeneity (thickness, etc.) or a metallurgical heterogeneity. The greater this heterogeneity, the more it tends to promote early initiation from the point of view of the average equivalent deformation of the structure.
- *Propagation of the crack*: Two phases can be distinguished: a stable phase and an unstable phase with much higher crack propagation velocities. The stable phase alone seems to be affected by the parameters of the design of experiment. The dominant parameter is the degree of heterogeneity which causes the initiation. The greater the heterogeneity, the slower the propagation. The second parameter is the test temperature. The higher the temperature, the faster the propagation in the stable phase. The volume of gas has an influence only if the depressurization kinetics is dominant versus the fracture kinetics (the high-heterogeneity case).

The design of the experiment showed no influence whatsoever of the 16MnNiMo5 steel grade on the results in terms of creep, crack initiation or crack propagation, even though, from a local point of view (observation of the fracture pattern), the relative brittleness of the Krakatoa grade compared to the Rupther grade was confirmed. Indeed, the influence of the grade is negligible compared to the influence of the strain and damage state of the structure when the crack-inducing instability occurs. That would not have been the case for tests on a pre-cracked structure, in which the damage responsible for the crack's propagation is localized at the crack's tip (the case of tests on CT specimens, which pointed out a great influence of the steel grade on the surface energy release rate Γ_0; Tardif et al., 2010).

Acknowledgements

The authors would like to thank the *Institut de radioprotection et de sûreté nucléaire* of Fontenay aux Roses (France) and the *Commissariat à l'énergie atomique* of Saclay (France) for their financial support and for providing the 16MnNiMo5 steel grades.

References

Bechta, S., Granovsky, V., Khabensky, V., Gusarov, V., Almiashev, V., Mezentseva, L., Krushinov, E., Kotova, S.Y., Kosarevsky, R., Barrachin, M., Bottomley, D., Fichot, F., Fischer, M., 2008. Corium phase equilibria based on MASCA, METCOR and CORPHAD results. Nuclear Engineering and Design 238, 2761–2771.

Bentz, Humphries, Chu, 2000a. Data Report For OLHF-1 Experiment. Tech. Rep.

Bentz, Humphries, Chu, 2000b. Results Of The OLHF Material Property Testing Program For SA533B1 Steel. Tech. Rep.

Bucalossi, 2001a. Common Result Report OCDE LHF Benchmark. Tech. Rep.

Bucalossi, 2001b. Summary Of The Activity Performed By AVN In The Framework Of The OCDE-LHF Benchmark. Tech. Rep.

Chu, T.Y., et al., 1998. Lower Head Failure Experiments and Analyses. Tech. Rep. Report NUREG/CR-5582, SAND98-2047.

Gentzbittel, J., Vincent, D., Cayron, C., 2007. Étude de la variabilite' des microstructures et des propriétés de rupture d'aciers 16MND5-Rapport Technique DTH/DL/2007/93. Tech. Rep., CEA/DTH/DL.

Gentzbittel, J.M., Calapez, J., 2008. Caractérisation de traction complémentaire des aciers Krakatoa et Rupther. Tech. Rep., LTH/DL/2008/13 CEA.

Griffith, A., 1920. The phenomena of rupture and flow in solids. Philosophical Transactions of Royal Society of London 221A, 163–198.

Humphries, L.L., et al., 2002. OECD Lower Head Failure Project Final Report. Tech. Rep. Report OECD/NEA/CSNI/2(2002)27, OECD.

Koundy, V., Caroli, C., Nicolas, L., Matheron, P., Gentzbittel, J.M., Coret, M., 2008a. Study of tearing behaviour of a PWR reactor pressure vessel lower head under severe accident loadings. Nuclear Engineering and Design 238, 2411–2419.

Koundy, V., Fichot, F., Willschuetz, H.G., Altstadt, E., Nicolas, L., Lamy, J.S., Flandi, L., 2008b. Progress on PWR lower head failure predictive models. Nuclear Engineering and Design 238, 2420–2429.

Nicolas, L., Mongabure, P., Ber, L.L., Devos, J., 2001. Comparison of the predictions relying on coupled/uncoupled damage-viscoplasticity models for creep test analyses. Journal of Pressure Vessel Technology 123 (3), 298–305.

OECD (Ed.), October 1993. Three Miles Island Reactor Pressure Vessel Investigation Project, Achievements and Significant Results. OECD, OECD.

OLIS (Ed.), June 2002. OLHF Seminar 2002. OECD, Madrid.

Sehgal, B., et al., 2003. Assessment of reactor vessel integrity (ARVI). Nuclear Engineering and Design 221, 23–53.

Sehgal, B., et al., 2005. Assessment of reactor vessel integrity (ARVI). Nuclear Engineering and Design 235, 213–232.

Seiler, J., Tourniaire, B., Defoort, F., Froment, K., 2007. Consequences of material effects on in-vessel retention. Nuclear Engineering and Design 237, 1752–1758.

Sestier, K., 1998. Evolution microstructurale et comportement mécanique à haute température de l'acier de cuve 16MND5 en situation d'accident grave. PhD thesis, Institut National Polytechnique de Grenoble.

Stampfl, J., Kolednik, O., 2000. The separation of the fracture energy in metallic materials. International Journal of Fracture 101 (321), 345.

Tardif, N., 2009. Étude du comportement á haute température d'une fissuration instable dans l'acier 16MND5 et application au calcul de la rupture d'un fond de cuve en cas d'accident grave. PhD thesis, Institut National des Sciences Appliquées de Lyon.

Tardif, N., Combescure, A., Coret, M., Matheron, P., 2010. Stable crack propagation in steel at 1,173 K: experimental investigation and simulation using 3D cohesive elements in large displacements. Engineering Fracture Mechanics 77, 776–792.

Turner, C.E., Kolednik, O., 1994. A micro and macro approach to the energy dissipation rate model of stable ductile crack growth. Fatigue & Fracture of Engineering Materials & Structures 17 (1089), 1107.

Vereecke, B., 2004. Une analyse probabiliste du comportement d'une famille d'aciers pour cuve de REP en cas d'accident grave. PhD thesis, Université Pierre et Marie Curie.